Nonisotropic Excitation Energy Transport in Organized Molecular Systems: Monte Carlo Simulation-Based Analysis of Fluorescence and Fluorescence Anisotropy Decay

Mikalai M. Yatskou,[†,‡] Harry Donker,[†] Eugene G. Novikov,[‡] Rob B. M. Koehorst,[†] Arie van Hoek,[†] Vladimir V. Apanasovich,[‡] and Tjeerd J. Schaafsma*[,†]

Laboratory of Biophysics, Department of Agrotechnology and Food Sciences, Wageningen University, Dreijenlaan 3, 6703 HA Wageningen, The Netherlands, and Department of Systems Analysis, Belarusian State University, 4, F. Scoryna Avenue, Minsk, 220050, Belarus

Received: December 7, 2000; In Final Form: July 23, 2001

An improved application is presented of the Monte Carlo method including simultaneous parameter fitting to analyze the experimental time-resolved fluorescence and fluorescence anisotropy decay of two organized molecular systems exhibiting a number of different, nonisotropic energy transfer processes. Using physical models and parameter fitting for these systems, the Monte Carlo simulations yield a final set of parameters, which characterize the energy transfer processes in the investigated systems. The advantages of such a simulation-based analysis for global parametric fitting are discussed. Using this approach energy transfer processes have been analyzed for two porphyrin model systems, i.e., spin-coated films of zinc tetra-(octylphenyl)-porphyrins (ZnTOPP) and the tetramer of zinc mono(4-pyridyl)triphenylporphyrin (ZnM(4-Py)TrPP). For the ZnTOPP film energy transfer rate constants of $\sim 1 \times 10^{12}$ s^{-1} and $\sim 80 \times 10^{9}$ s^{-1} have been found, and are assigned to intra- and interstack transfer, respectively. For the tetramers, the transfer rate constants of 38×10^{9} and 5×10^{9} s^{-1} correspond to energy transfer to nearest and next nearest neighbor molecules, respectively. The results are in agreement with a Förster type energy transfer mechanism.

1. Introduction

Energy transport, in the following denoted as E.T., in organized molecular systems is one of the most important processes in photosynthesis, optoelectronic devices, artificial light harvesting systems, and solar cells.[1−5] The unique property of E.T. in photosynthetic complexes is its high efficiency even though this transfer occurs over relatively long distances. The reasons for this high efficiency are currently only partly understood.

E.T. processes in various natural pigment complexes and synthetic assemblies of chromophores have been widely studied through time-resolved fluorescence and fluorescence anisotropy measurements.[6−9] Although a number of analytical expressions have been developed describing energy transfer phenomena observed via time-resolved fluorescence and fluorescence anisotropy decay, mostly these expressions are unsuitable for complex, nonisotropic molecular systems, e.g., linear molecular aggregates in solution, liquid crystals, and solid films containing ordered domains.[10−14] One of the efficient nonanalytical methods which in principle can describe the E.T. processes in complex systems, including nonisotropic ones, is the Monte Carlo (in the following denoted as M.C.) simulation method.[7,15,16] Although this method has been used extensively to test the validity of the approximations made in analytical theories,[17−20] its possibilities stretch much further, as is demonstrated in this work.

Modeling E.T. processes in molecular assemblies using M.C. simulations has the advantage—among others—that it gives direct insight how various parameters of the model affect the experimental characteristics of the system, e.g., the time dependence of the anisotropy spectrum. Recently, M.C. algorithms have been applied to several types of E.T. mechanisms in nonisotropic molecular systems.[10,12,19] These algorithms need to assume a priori a particular type of E.T., i.e., by a Förster, higher multipole or exchange mechanism.[6,21,22] Often, in systems with donor−acceptor distances comparable to the molecular dimensions, such an a priori assumption cannot be made, however, since it is then unclear to what extent each mechanism contributes to the observed E.T. rate constants. Another common problem concerns those systems where analytical expressions lead to undistinguishable results or are too complicated to provide clear evidence for a dominant energy transfer mechanism.[14]

We present an improved method to investigate E.T. processes in ordered, nonisotropic molecular systems, based on the parameter fitting via M.C. simulations,[23,24] which does not require the type of E.T. mechanism to be known beforehand, and includes the analysis of statistical noise to judge the quality of the fit. The presented method has also been applied to analyze the time dependence of the fluorescence anisotropy. Previous application[10,12,19] of the M.C. method to fluorescence decay of organized systems did not include or discuss some of these aspects in such detail.

There are at least four steps to be taken in this approach: (i) create a physical model (which includes the geometry, dynamics, etc.) of the investigated molecular system, (ii) develop and program a simulation model based on the physical model, with the model parameters corresponding to the various kinetic characteristics of the molecular system, (iii) find through parametric fitting an optimum set of parameters of the simulation model corresponding to the experimental data, (iv) calculate

* Corresponding author. Tel: +31-317482044. Fax: + 31-317482725. E-mail: Tjeerd.Schaafsma@mac.mf.wau.nl.
[†] Laboratory of Biophysics.
[‡] Department of Systems Analysis.

10.1021/jp0044227 CCC: $20.00
Published on Web 09/22/2001

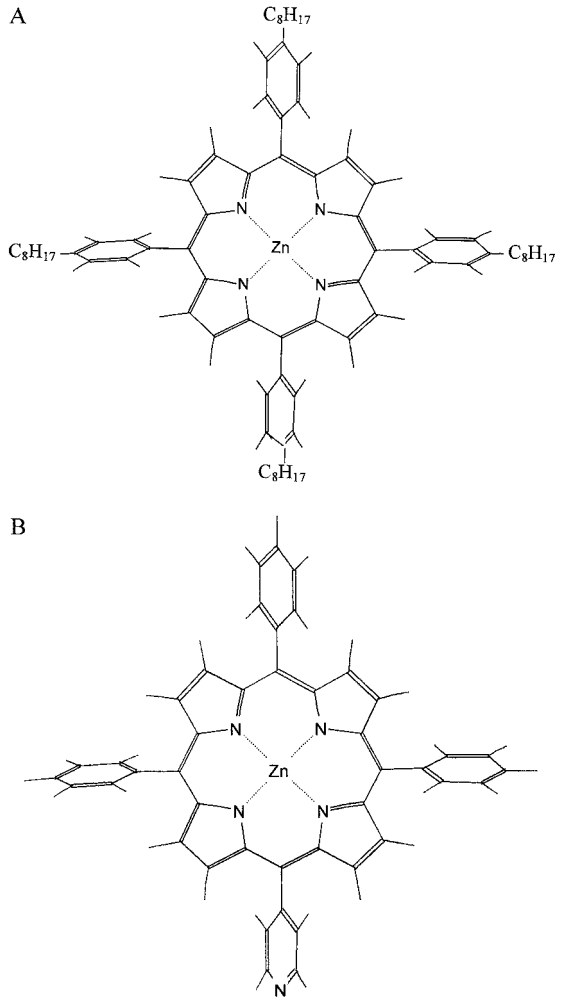

Figure 1. Structures of ZnTOPP (A) and Zn(4-Py)TrPP (B).

the reduced χ^2 value for a quantitative determination of the accuracy of the simulated decay curve.

This paper describes in detail how the kinetic constants for E.T. between the components of nonisotropic molecular systems, i.e., for two different porphyrins, can be determined using M.C. parameter fitting. Porphyrins belong to a widely studied class of compounds that can form ordered structures,[25−29] and thereby should be expected to exhibit nonisotropic E.T. We consider two porphyrin systems, for which an analytical description of the E.T. process can hardly be derived from general principles and thus M.C. simulations might be useful.

The first porphyrin model system (further denoted as **system 1**) consists of ≤100 nm thick, spin-coated films of a self-organizing porphyrin, ZnTOPP (Figure 1A), on quartz substrates, that have intentionally been doped with known amounts of an effective fluorescence quencher, i.e., copper tetra(-octylphenyl)-porphyrin (CuTOPP). A spectroscopic study of these films[30] has shown that the films consist of layers built from one-dimensional stacks of porphyrins with a "slipped deck of cards" configuration. The stacks are oriented with their short axes perpendicular to the substrate, whereas their long axes are distributed randomly in the plane parallel to the substrate, most likely in ordered domains. Time-resolved fluorescence measurements have shown that the fluorescence decay is not a single exponential, indicating E.T. inside the film. Analysis of the fluorescence decay using analytical models has also shown that the E.T. process (shown to be of the singlet type) is best described by a quasi one-dimensional diffusion-limited model.[31,32] Such an analytical model only yields a rough estimate of the rate constant for intrastack energy transfer but not for the interstack process. Finally, the application of the analytical model led to the conclusion that undoped ZnTOPP films contain a significant amount of nonintentional traps. Again, only a rough estimate could be given of the concentration of these traps. The present work demonstrates that more accurate and detailed information about the E.T. processes and the trap concentration can be obtained using M.C. simulations.

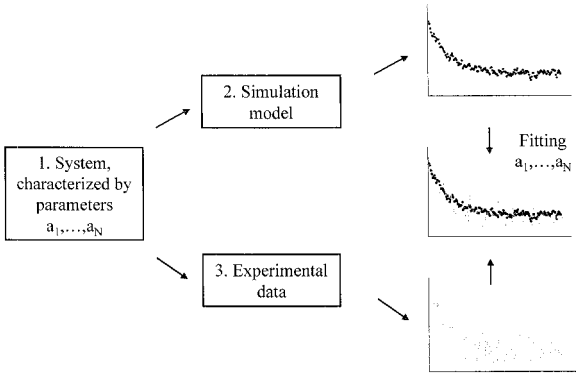

Figure 2. Simulation approach by parametric fitting.

The second model system (further denoted as **system 2**) is the tetramer of Zn(4-Py)TrPP (Figure 1B), in toluene solution.[33] Contrary to what has been observed for ZnTOPP films, the tetramer fluorescence decay of $[Zn(4\text{-Py})TrPP]_4$ is a single exponential, which reflects the kinetics of the lowest singlet excited-state S_1 of ligated Zn(4-Py)TrPP.[33] Since the porphyrin units in the tetramer are identical, energy transfer processes occurring between these units can only show up in the fluorescence anisotropy. Although the fluorescence anisotropy can in principle be analyzed by one of the proposed algorithms,[19,34,35] the distances between the porphyrin units in the tetramer are comparable to the porphyrin diameter and therefore an a priori choice for a dominant mechanism of energy transfer is not justified. It could be argued that the exchange mechanism does not apply as a result of the perpendicular orientation of the porphyrin monomers. That may not be true, however, if the monomers in the tetramer are not perfectly flat, i.e., do not have D_{4h} symmetry, e.g., by distortion of the monomers as a result of the mutual ligation of the monomers in the tetramer. As is shown by this work, the energy transfer rate constants as well as the transfer mechanism for the tetramer can be determined by M.C. simulation.

2. Simulation Approach

2.1. Parametric Fitting via Monte Carlo Simulations. Parametric fitting using M.C. simulations is schematically presented in Figure 2. The method approximates the experimental data (**block 3**) by the synthetic data (**block 2**) simulated using the M.C. methods.[7,15,16] Assuming that the theoretical model with the least number N of system parameters $\mathbf{a} = \{a_1,...,a_N\}$ unambiguously describes the system (**block 1**), the best approximation of the experimental data yields the values of **a**. The best approximation is defined by a criterion (or set of criteria), establishing how far the simulated fluorescence decay deviates from the experimental data. Generally, such a criterion is analytically represented by a function of the experimental and simulated data and is strongly dependent on the particular application area, the particular simulation method and the experimental conditions. In our numerical experiments we use the following criterion

$$\chi^2(\mathbf{a}) = \sum_{i=1}^{n} \frac{[F^{\mathrm{E}}(t_i) - F^{\mathrm{T}}(t_i,\mathbf{a})]^2}{w(t_i)} \quad (1)$$

where n is the number of channels of the multichannel analyzer ($N \ll n$); $w(t_i)$ is the weighting factor; $F^{\mathrm{E}}(t_i)$ is the experimental fluorescence decay, represented by the number of detected counts per channel; and $F^{\mathrm{T}}(t_i,\mathbf{a})$ is the *simulated fluorescence decay*, represented by the number of simulated counts per channel. According to this criterion the best approximation, corresponding to the set of parameters **a**, is that which yields a minimum for $\chi^2(\mathbf{a})$. Although the criterion $\chi^2(\mathbf{a})$ in eq 1 is similar to that widely applied in statistics as the χ^2 criterion,[36,37] the expression 1 differs from that commonly used, since both $F^{\mathrm{T}}(t_i,\mathbf{a})$ and $F^{\mathrm{E}}(t_i)$ contain statistical noise.

Fortunately, the statistical characteristics of the noise in the experimental data, as well as in the simulation model, are often known. For our case, all measurements were made using the time-correlated single photon counting (TCSPC) method and streak camera detection, respectively, where the number of counts per channel of the multichannel analyzer is well approximated by Poisson statistics.[38,39] If the amount of experimental data is large enough ($> \sim$30 counts per channel) the Poisson statistics transforms into Gaussian statistics.[38,39] Since the simulation model can be reproduced with an a priori statistical preciseness which is the same as, for instance, for the molecular behavior under the same conditions as in the experiments, the same statistics can be made to apply to the simulated data of $F^{\mathrm{T}}(t_i,\mathbf{a})$.

Under the present conditions the statistical characteristics of the χ^2 criterion are directly applicable to eq 1. Indeed, the numerator $[F^{\mathrm{E}}(t_i) - F^{\mathrm{T}}(t_i,\mathbf{a})]$ of eq 1 is the difference between two Gaussian random variables. This difference itself is also the random variable of a Gaussian distribution with a zero mean value and a variance given by

$$w(t_i) = \mathrm{var}[F^{E}(t_i) - F^{T}(t_i,\boldsymbol{a})] = \mathrm{var}[F^{E}(t_i)] + \mathrm{var}[F^{T}(t_i,\boldsymbol{a})] \quad (2)$$

where it is assumed that $F^{\mathrm{E}}(t_i)$ and $F^{\mathrm{T}}(t_i,\mathbf{a})$ are statistically independent and that $F^{\mathrm{T}}(t_i,\mathbf{a})$ represents the best approximation for the experimental data $F^{\mathrm{E}}(t_i)$. Using eq 2 as a weighting factor $w(t_i)$ in eq 1, the latter becomes a sum of squares of n independent standard Gaussian variates and can be described by a χ^2 density distribution function. Therefore, it should be expected that the mean value of a random variable of $\chi^2(\mathbf{a})$ equals the number of degrees of freedom $\nu = n - N - 1$, and the variance of a random variable of $\chi^2(\mathbf{a})$ equals ν. In the following we will use the normalized value $\chi^2(\mathbf{a})/\nu$ of $\chi^2(\mathbf{a})$.

If the number of counts per channel in the theoretical histogram approaches infinity, then the variance $\mathrm{var}[F^{\mathrm{T}}(t_i,\mathbf{a})]$ vanishes, and we arrive at the commonly used representation of the χ^2 criterion. In practice, we are able to increase the number of simulated counts as much as the computer facilities allow us to do, thus ensuring higher accuracy for the theoretical function.

Note that, although many papers nicely describe the application of the M.C. method to different molecular systems exhibiting E.T.,[7,9,10,12,19] all of them require a set of a priori known parameters, which define the system structure and functionality. In our method we employ the same type of simulation models but with a set of unknown input parameter values. The correct values (or their estimates) are found through parametric fitting of the experimental data.

2.2. Global Analysis. M.C. simulation monitored by the parametric fitting procedure opens the way for the application of the global analysis approach to a wide variety of research fields. The method commonly consists of fitting a set of measured responses by a corresponding set of theoretical models. Certain parameters of the theoretical models can be linked, for example, by forcing these parameters to be equal for all synthetic curves of the set.

In a more general approach a multidimensional experimental surface (for example, the fluorescence response, measured at different times, excitation/emission wavelengths, concentrations, temperatures, polarization angles, etc.) is fitted by the corresponding multidimensional theoretical model with a common set of unknown parameters. Such theoretical models are built on the basis of general physical laws. As a consequence there is no need to equalize particular parameters. This way of analysis ensures a consistent picture of the processes under investigation.

To build such a theoretical response in a multidimensional space is a rather tedious task using analytical techniques. The problems inherent to this approach are at least 2-fold: (i) obtaining the analytical description of the processes, often represented by integral or differential equations, and (ii) technical problems of numerical implementation inherent to handling multidimensional arrays of numbers, which usually is very time- and memory-consuming even on modern computers. If, according to the model, one needs to solve integral or differential equations in multidimensional space, it most likely slows down the calculations considerably.

On the other hand, a M.C. simulation model operates by the elementary processes, which are easy to understand and to program. As a rule, no sophisticated mathematical methods are required: the simulation algorithm reproduces the physical processes occurring in the system almost directly. Moreover, the generation of a multidimensional theoretical function in the case of E.T. is rather straightforward. If, for example, one simulates the effects of E.T. in a time-resolved fluorescence experiment, each excitation photon is considered as an object having time- and space coordinates, a polarization vector, an energy, etc. In the simulation procedure, those parameters can be introduced with the required precision. Simultaneously, the desired statistical characteristics can be recorded, thus resulting in a defined multidimensional response.

We finally note that the M.C approach used in the experimental data analysis is somewhat similar to the M.C. methods widely used in numerical analysis.[15,16,40,41] For example, multidimensional integration, performed using the methods of Monte Carlo often allows one to save computer memory and, eventually, CPU time.

2.3. Simulation of the Time-Resolved Fluorescence and Anisotropy. In the following paragraphs we describe the basic principles underlying the simulation of fluorescence and fluorescence anisotropy decay. Since each photon can be simulated as an object having a time coordinate and a polarization vector, the simulation model can generate simultaneously both the fluorescence and the anisotropy decays.

The experimental procedure includes the determination of the components of the detected fluorescence, which are differently polarized with respect to the polarization direction of the excitation light. Figure 3 schematically represents the basic principles of the detection of the parallel ($I_{\parallel}$) and perpendicularly ($I_{\perp}$) polarized fluorescence components, corresponding to the detection using a polarizer oriented at 0° and 90° wrt the polarization direction of the excitation light, denoted as the z-direction. A molecule can absorb an excitation photon with a

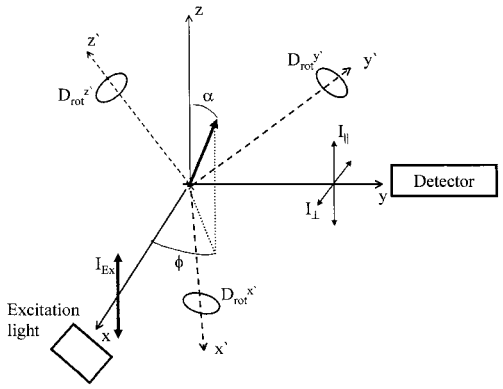

Figure 3. Schematic diagram for the measurement and simulation of parallel and perpendicularly polarized fluorescence components. α: angle between the transition moment for emission and the direction of the parallel detector. ϕ: angle between the projection of the emission transition moment onto the *xy* plane and the *x* axis.

probability that is proportional to the square of the cosines of the angle between the polarization vector of the excitation photon and one or more absorption transition moments of a molecule.[17] Note that usually for isotropic systems a molecular coordinate system (x',y',z') is randomly oriented in a fixed laboratory coordinate system (x,y,z). This may be incorrect for nonisotropic molecular systems, however, since the molecular coordinate system can be either fixed or nonrandomly distributed relative to the laboratory coordinate system. After being excited, a molecule remains in an excited state for a random time interval Δt_τ, defined by the exponential probability density function with a mean value equal to the fluorescence lifetime τ. Subsequently, a molecule can emit a photon in any direction, but we are interested in the x and z directions only, since $I_{||}$ and $I_\perp$ are detected along these two axes. Detecting the $x(I_{||})$ and $z(I_\perp)$ components of the emitted photons, the total fluorescence and anisotropy can be represented by the following equations

$$I(t) = I_{||}(t) + 2I_\perp(t) \tag{3}$$

$$r(t) = \frac{[I_{||}(t) - I_\perp(t)]}{[I_{||}(t) + 2I_\perp(t)]} \tag{4}$$

Figure 4 shows a flow diagram of the algorithm for simulation of the $I_{||}(t)$ and $I_\perp(t)$ components of the time-resolved fluorescence. The simulation procedure starts in **block 1** by setting the number N_R of simulation runs (or excitation photons) and generating the initial orientations Ω_0^a and Ω_0^e of the absorption and emission transition dipole moments, characterized by the azimuth and polar angles with respect to the laboratory system. The full travel of a single photon, starting from the excitation of the molecular system and finishing by the photon emission, is considered as one simulation run. Employing an excitation-hopping model for the E.T. in **block 2** we simulate a time interval Δt_{ET} and the orientation $\Omega^e(\alpha,\phi)$ of the emission transition dipole moment after several transfer hops and diffusional rotations of the molecular system. Particular excitation-hopping models for **systems 1** and **2** will be considered in sections 4.1.2 and 4.2.2, respectively. A time shift Δt_e due to the finite width of the excitation pulse and delays in the detector is simulated in **block 3** using the experimentally measured instrumental time response function $E(t)$ representing the convolution of the shape of laser pulse and the detector response. The algorithm of generating a time shift Δt_e can be implemented in several ways.[42−44] Since $E(t)$ is an experimentally measured function, we use the numerical algorithm based on the Neumann

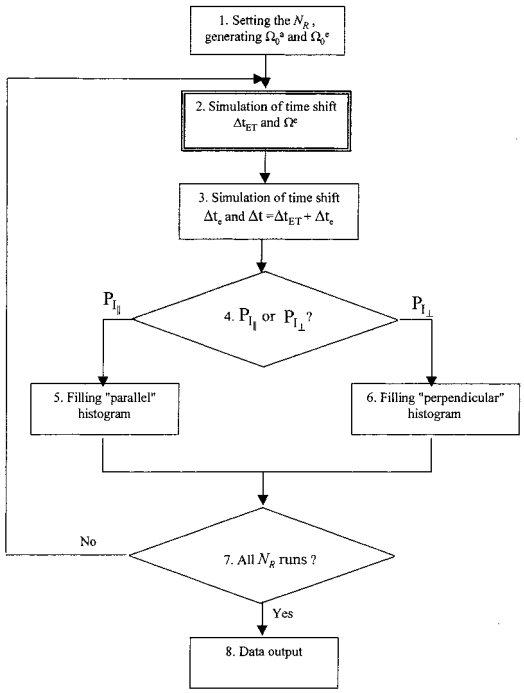

Figure 4. Flow diagram of the simulation algorithm for the $I_{||}(t)$ and $I_\perp(t)$ components of the time-resolved fluorescence. Photons are represented as discrete events or particles, which can be found in particular states, e.g., being parallel or perpendicularly polarized, and having a certain time and/or space localization. Therefore, each photon possesses either perpendicular or parallel polarization (with a certain probability) and it contributes to either the $P_\perp$ or $P_{||}$. The contribution of the emitted photon to the $I_{||}(t)$ or $I_\perp(t)$ in block 4 is calculated using eqs 5 and 6.

method.[45] To apply this algorithm we first normalize $E(t)$, so that $\int_{0+}^{\infty} E'(t)\, dt = 1$ where $E'(t) = E(t)/A$ and A is the normalization factor. After the normalization, the instrumental time response function $E'(t)$ represents a probability density function which can be directly used in the Neumann simulation procedure. To avoid possible fitting problems, caused by the different numbers of photon counts for the experimental and simulated decays, we apply the same normalization procedure for both experimental and simulated decays. Thus, after several simulation steps, the total time shift $\Delta t = \Delta t_{ET} + \Delta t_e$ is recorded in **blocks 5** or **6** as belonging to either the "parallel component" ($P_{I||}$) or the "perpendicular component" ($P_I\perp$) histograms, respectively, using the following equations[8]

$$P_{I_{||}} \sim \cos^2 \alpha \tag{5}$$

$$P_I\perp \sim \sin^2 \phi \sin^2 \alpha \tag{6}$$

The angles α and ϕ are determined by the density distribution function $f(\alpha,\phi)$ of the emission transition moment around the x, y, and z coordinate axes, by the molecular geometry as it affects the diffusion coefficients for rotation $D_{rot}^{x'}$, $D_{rot}^{y'}$, and $D_{rot}^{z'}$, by the angle between the absorption and emission transition moments, and by the energy transfer process itself.[46] Simulation runs (**blocks 2**−**4**) are repeated N_R times (**block 7**). Finally, both histograms are used to calculate the simulated fluorescence and anisotropy decays using eqs 3 and 4.

The presented simulation model encompasses the case when the position of the detector in the laboratory system is not included into the eqs 5 and 6. In principle, the detector can be oriented at any steric angle $\delta^{Det} = (\alpha^{Det},\phi^{Det})$ with respect to the laboratory coordinate system. Then the probability to detect

the emitted photon in the direction δ^{Det} is proportional to the radiation intensity in the δ^{Det} direction and equals $^3/_2 \sin^2 \gamma$,[17] where γ is an angle between the emission dipole moment and the polarization angle of the detector. Then, eqs 5 and 6 take the form:

$$P_{I_{||}} \sim {}^3/_2 \sin^2\gamma \cos^2\alpha = {}^3/_2 [1 - (\cos\alpha \cos\alpha^{Det} + \sin\alpha \cos\phi \sin\alpha^{Det} \cos\phi^{Det} + \sin\alpha \sin\phi \sin\alpha^{Det} \sin\phi^{Det})^2] \cos^2\alpha \quad (7)$$

$$P_I\perp \sim {}^3/_2 \sin^2\gamma \sin^2\phi \sin^2\alpha = {}^3/_2 [1 - (\cos\alpha \cos\alpha^{Det} + \sin\alpha \cos\phi \sin\alpha^{Det} \cos\phi^{Det} + \sin\alpha \sin\phi \sin\alpha^{Det} \sin\phi^{Det})^2] \sin^2\phi \sin^2\alpha \quad (8)$$

If the detector is oriented in the *y* direction, as in Figure 3, i.e., $\alpha^{Det} = 90°$ and $\phi^{Det} = 90°$, then eqs 7 and 8 simplify to

$$P_{I_{||}} \sim {}^3/_2(1 - \sin^2\alpha \sin^2\phi) \cos^2\alpha \quad (9)$$

$$P_I\perp \sim {}^3/_2(1 - \sin^2\alpha \sin^2\phi) \sin^2\phi \sin^2\alpha \quad (10)$$

In general the shape of the optical spectra can be simulated as well using the above-mentioned mathematical algorithms.

3. Experimental Section

3.1. Chemicals. Zinc tetraphenylporphyrin (ZnTPP), ZnTOPP and ZnM(4-Py)TrPP were prepared by metallization of free base tetraphenylporphyrin (H_2TPP) free base tetra-(octylphenyl)-porphyrin (H_2TOPP) and free base mono(4-pyridyl)-triphenylporphyrin (H_2M(4-Py)TrPP), respectively, by refluxing in DMF with $ZnCl_2$ (Merck, p.a.). CuTOPP was synthesized by the same procedure using $CuCl_2 \cdot 2H_2O$ (Merck, p.a.).[47] H_2TPP, H_2TOPP and H_2M(4-Py)TrPP were synthesized by condensation of benzaldehyde, 4-(*n*-octyl)benzaldehyde and a mixture of benzaldehyde and 4-pyridinecarbaldehyde, respectively, with pyrrole (Janssen Chimica, 99%) in refluxing propionic acid (Merck, z.s.).[48,49] The porphyrins were purified by chromatography on silica (Merck, silica gel 60) with toluene (ZnTOPP, CuTOPP) or chloroform (ZnTPP, ZnM(4-Py)TrPP) as eluent. All porphyrins are estimated to be >99% pure as shown by thin-layer chromatography and absorption, fluorescence spectroscopy.

Preparation of Porphyrin Films for the System 1. Thin films of ZnTOPP doped with various concentrations of CuTOPP as well as undoped films on quartz plates (Suprasil, ∅ 15 mm and 1 mm thickness) were prepared by spin coating from 5×10^{-5} M toluene solutions. As the solutions already contained the appropriate amounts of ZnTOPP and CuTOPP, it may be assumed that in the films the CuTOPP molecules are distributed statistically among the ZnTOPP molecules. Before spin coating the quartz plates were subsequently rinsed with aqua regia, water, methanol, and toluene and blown dry with nitrogen. For duplicate samples ZnTOPP purchased from Porphyrin Products were used. Results obtained with purchased or home-synthesized ZnTOPP were identical.

Preparation of Solutions for System 2. Solutions of the 10^{-5} M ZnM(4-Py)TrPP in toluene were prepared after drying with sodium wire and stored over molecular sieves.

3.2. Time-Correlated Photon-Counting Setup. The experimental setup for TCSPC has been described in detail elsewhere.[30,50,51] A mode-locked continuous wave Nd:YLF laser (Coherent model Antares 76-YLF, equipped with a LBO frequency doubler (Coherent model 7900 SHGTC) and BBO frequency tripler (Coherent model 7950 THG) was used to synchronously pump a continuous wave dye laser (Coherent radiation model CR 590). As a dye Coumarin 460 was used for excitation at 465 nm. A setup with electrooptic modulators in a dual pass configuration was used to reduce the pulse rate to 594 kHz.[52] The final pulse duration of the excitation pulses was ~4 ps fwhm, and the maximum pulse energy was ~100 pJ. The spin-coated samples were fixed on a thermostated, spring-loaded holder at an angle of 15° with respect to the direction of excitation.

Fluorescence light was collected at an angle of 90° with respect to the direction of the exciting light beam. Between the sample and the photomultiplier detector were placed: a set of single fast lenses with a rotatable sheet type polarizer between, followed by a monochromator and a second set of single fast lenses focusing the output light of the monochromator on the photomultiplier cathode. All lenses were uncoated fused silica, F/3.0. The polarizer sheet was in a dc motor driven ball-bearing holder with mechanical stops, allowing computer-controlled rotation (0.2 s). The sheet polarizer was Polaroid type HNP′B. The emission was detected, polarized under magic angle. The detection monochromator was a CVI model Digikröm 112 double monochromator (F/3.9) with the two gratings placed in a subtractive dispersion configuration. Because of the low intensity, wide slits ($\Delta\lambda$ = 16 nm) were used. Detection electronics were standard time correlated single photon counting modules. The presented data were collected in a multichannel analyzer (MCA board from Nuclear Data model AccuspecB, in a PC) with a time window of 8192 channels at 3.125 ps/channel.

By reducing the intensity of the excitation pulses, a maximum photon frequency of 30 kHz (≈5% of 594 kHz) was chosen[53] to prevent pile-up distortion. Also, other instrumental sources for distortion of data were minimized[54] to below the noise level of normal photon statistics. Extreme care was taken to prevent artifacts from background luminescence. All substrates were carefully cleaned and checked for background luminescence prior to the measurements. For samples with a low fluorescence yield, the background luminescence of an uncoated substrate was recorded and subtracted from the sample data in analysis. For obtaining a dynamic instrumental response (~50 ps fwhm) for deconvolution purposes, the scatter of a rough-hewn, uncoated quartz substrate of 1 mm thickness was measured at the excitation wavelength.

3.3. Streak Camera. The experimental setup for the streak camera has previously been described.[55] The solution of ZnM-(4-Py)TrPP in toluene was excited with 100 fs pulses of 565 nm, selected for the tetramers, at 10 °C. The pulses were generated at a 125 kHz repetition rate using a titanium:sapphire-based oscillator (Coherent MIRA), a regenerative amplifier (Coherent REGA), and a double pass optical parametric amplifier (Coherent OPA-9400). The pulse energy was typically 25 nJ. The polarization of the exciting light was alternated between horizontal and vertical. The vertical component of the fluorescence was detected using a Hamamatsu C5680 synchroscan streak camera with a Chromex 250IS spectrograph. The full width at half-maximum (fwhm) of the overall time response of this system was 3.5 ps, and the spectral resolution was 8 nm. One streak image measured 315 nm in the spectral domain (1018 pixels) and 200 ps (1000 pixels) in the time-domain.

4. Analysis of Porphyrin Systems by M.C. Simulations

4.1. System 1. *4.1.1. Film Structure.* The porphyrin **system 1** consists of domains of ordered porphyrins on a quartz substrate

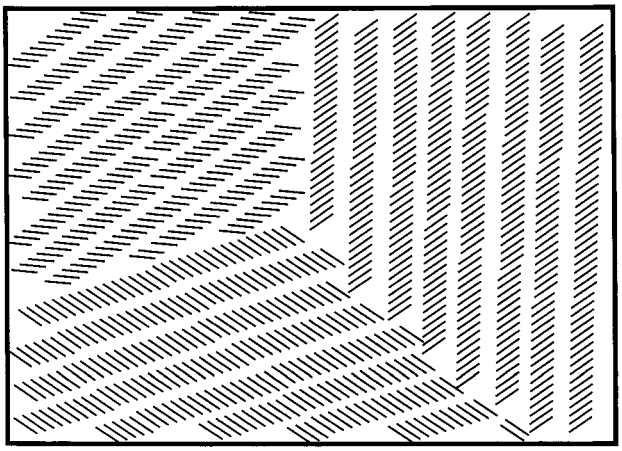

Figure 5. Two-dimensional molecular arrangement of ZnTOPP stacks spin-coated from toluene solution on a quartz substrate.

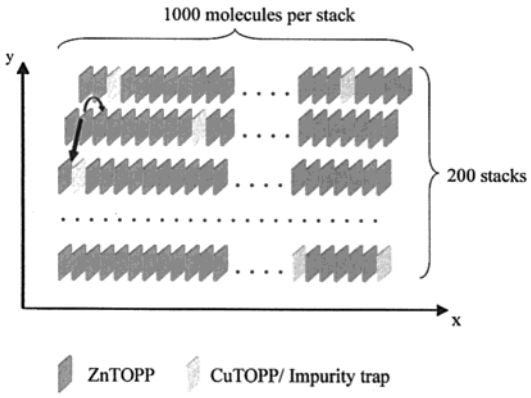

Figure 6. Domain arrangement of porphyrins for **system 1**. The arrows indicate the directions of energy transfer.

as shown in Figure 5. Within a particular domain the porphyrins are organized as a collection of stacks with their long axes oriented with respect to the domain axis.[30] There are two types of molecules in this system which are involved in energy transfer: (i) ZnTOPP and (ii) CuTOPP. The energy transport in this system can be studied through the ZnTOPP fluorescence as CuTOPP acts as a dark energy trap, quenching the ZnTOPP fluorescence. Also the presence of nonintentional traps (non-eliminated impurity molecules) results in quenching of the ZnTOPP fluorescence. The molar fraction N_{CuTOPP} of CuTOPP was 0, 1×10^{-2}, 2×10^{-2}, and 3×10^{-2}, and the fraction N_{imp} of nonintentional impurity molecules was constant under the experimental conditions. Under these conditions energy transfer between separated domains and singlet−singlet annihilation are assumed to be negligible.

4.1.2. Simulation Model. The simulation model for **system 1** is built on the basis of a single 2D domain model of porphyrin stacks approximated by the field of 1000×200 molecular sites in the (x,y) plane, parallel to the substrate surface, which is assumed to be atomically flat (Figure 6). The 1000×200 field has been chosen to combine a reasonably large domain size with a practical CPU time. The parameters k^x_{ET} and k^y_{ET} represent the E.T. rate constants in the x and y directions, and τ is the fluorescence lifetime of isolated monomeric ZnTOPP in the film. We applied a 2D domain E.T. model since (i) the ZnTOPP layers have a lamellar structure[56,57] and (ii) it is in better agreement with the results of a multiexponential analysis of the fluorescence and fluorescence anisotropy decay.[30] The parameters k^x_{ET}, k^y_{ET}, and τ^{-1} are proportional to the probabilities P^x_{ET}, P^y_{ET}, and P_τ, where $P^x_{ET} + P^y_{ET} + P_\tau = 1$, to be used in the simulation model.

We make the following assumptions: (i) the probabilities of the "left" and "right" E.T. are equal in both x and y directions for ZnTOPP and traps (CuTOPP). Furthermore, the probability for E.T. from excited ZnTOPP to a neighboring ground-state H_2TOPP trap is assumed to be 1, considering the relative energies of the lowest excited singlet state of ZnTOPP and H_2-TOPP, as well as the spectral overlap between the fluorescence and absorption spectra of both compounds; (ii) the probability of E.T. between nonneighboring molecules in a stack is at least one order smaller than that for transfer between neighboring porphyrin molecules; (iii) the probability of a jump in the y direction covers all possible ways of energy transfer in the y direction.

Summarizing, the simulation model is characterized by five parameters, i.e., k^x_{ET}, k^y_{ET}, N_{CuTOPP}, N_{imp}, and τ. A flow diagram for a single simulation run for **system 1** is presented in Appendix A.

4.1.3. Results and Discussion of Computer Simulations. The time-resolved fluorescence decays of ZnTOPP films (**system 1**) were analyzed using parametric fitting via Monte Carlo simulation models as described above. The number of channels in simulated histograms is 2048. For every simulation run, a time shift Δt_e was applied using the algorithm described in section 2.3.

Parametric fitting was applied based on the Nealder and Mead optimization method.[58] The fluorescence response of films containing 1×10^{-2}, 2×10^{-2}, and 3×10^{-2} molar fractions of CuTOPP was analyzed globally. Since the fluorescence decays measured for different concentrations of CuTOPP should have the same lifetime for isolated monomeric ZnTOPP and the percentage of nonintentional impurity, these parameters were global parameters linked through the fluorescence decays of porphyrin **system 1**, measured at different concentrations.

The statistical χ^2 criterion as well as the plots of the weighted residuals and the autocorrelation function were used to judge the quality of the fit. The 95% confidence intervals of the simulated decay parameters were calculated using the method of asymptotic standard errors.[59] All computer simulations were performed on a PC IBM Pentium III, 366 MHz.

To build up the theoretical fluorescence decay we used 10^8 simulation runs. On one hand this ensures an acceptable signal-to-noise ratio for the simulated decay, and on the other hand a reasonably short simulation time.

All experimental fluorescence decays could be satisfactorily fitted by the simulated decays. Figure 7 shows some typical fits of the experimental decay of ZnTOPP using the parameters in Table 1.

The intrastack energy transfer rate constant k^x_{ET} is found to be almost one order larger than that for the inter-stack transfer k^y_{ET}. The molar fraction N_{CuTOPP} of CuTOPP in the film is found to be in the same range as that of the porphyrin solution used for spin coating. From the simulation results we found $N_{imp} \sim 0.6 \times 10^{-2}$ molar fraction of impurity molecules to be present in addition to the dopant. The fluorescence lifetime τ of isolated monomeric ZnTOPP is close to the value of 1.81 ± 0.03 ns found in toluene solution in the absence of dopant or impurity.

In this paper we have limited ourselves to the fluorescence decay analysis of ZnTOPP films, yielding the E.T. rate constants by using M.C. simulations. Note that the E.T. rate constants resulting from the M.C. simulations of the fluorescence anisotropy decay of ZnTOPP films, which are not shown here, also

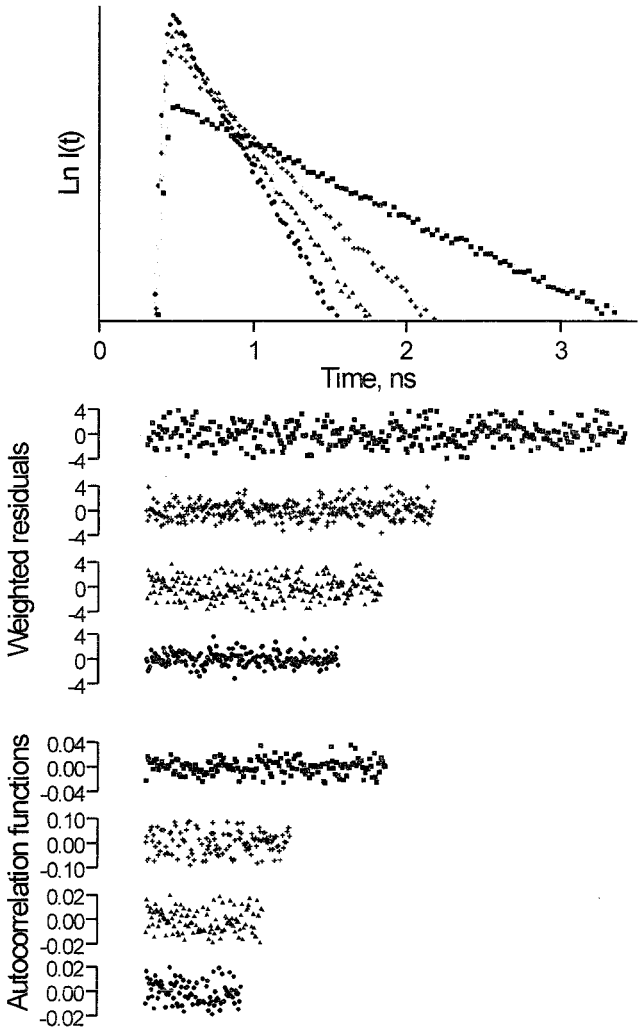

Figure 7. Fit of fluorescence decays of ZnTOPP in order of increasing rate constants, with molar fractions of CuTOPP: 0 (■, $\chi^2 = 1.18$), 1×10^{-2} (+, $\chi^2 = 1.10$), 2×10^{-2} (▲, $\chi^2 = 1.11$), and 3×10^{-2} (●, $\chi^2 = 1.08$). Simulated data are represented by solid lines. $\lambda_{exc} = 465$ nm; $\lambda_{det} = 580$ nm.

TABLE 1: Parameters and Their 95% Confidence Intervals[a] for Simulation-Based Fits of Experimental Decays of Systems 1 and 2

systems	τ^b(ns)	$N_{Imp}{}^b$ ($\times 10^{-2}$)	N_{CuTOPP} ($\times 10^{-2}$)	k^x_{ET} ($\times 10^{12}$ s^{-1})/ k^N_{ET} ($\times 10^9$ s^{-1})	k^y_{ET}/ k^A_{ET} ($\times 10^9$ s^{-1})
1	1.80	0.6	0.0	1.1	71
	[1.76;1.84]	[0.5;0.7]	[0.0;0.0]	[0.9;1.3]	[63;79]
			1.0	1.0	83
			[0.9;1.1]	[0.8;1.2]	[71;95]
			2.0	0.9	77
			[1.9;2.1]	[0.8;1.0]	[67;87]
			3.0	0.9	83
			[2.9;3.1]	[0.8;1.0]	[67;99]
2	1.50			38	5
	[1.45;1.55]			[33;43]	[0;6]

[a] In square brackets. [b] Simultaneous fit of lifetime and impurity levels using global analysis.

agree with the results from a multiexponential analysis of the fluorescence decay.[30]

The intra- and interstack E.T. rate constants following from the M.C. simulation cannot be compared in a straightforward manner with those calculated by the Förster or exchange type of E.T. since at the molecular level the optical properties of solid films, such as the refractive index or the permittivity

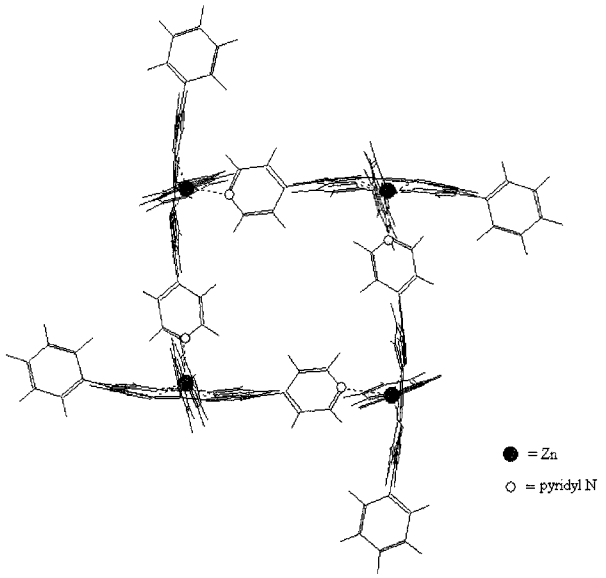

Figure 8. The tetrameric structure of [ZnM(4-Py)TrPP]$_4$.

coefficient, are not well-defined. However, we can qualitatively interpret the ratio (k^x_{ET}/k^y_{ET}) of E.T. parameters resulting from M.C. simulations by comparison with the theoretically calculated ratio (k^x_{ET}/k^y_{ET}) if we make an educated guess for the film structure, in particular for the intermolecular distances and the type of mechanism which gives rise to the energy transfer. The plane-to-plane distance between two molecules in a stack is estimated to be ≈5 Å, and that between two stacks to be ≈10−50 Å.[30] Considering the presence of octyl chains between stacks, for a close-packed structure of the porphyrin stacks in the film the interstack distance is estimated to be ≈11 Å. Even though this distance can only be estimated, it indicates that there is no significant overlap between the π-orbitals of any two porphyrin monomers of two neighboring stacks, and therefore E.T. by the exchange mechanism is expected to be negligibly small. At the same time, we cannot completely exclude exchange mechanism from intrastack E.T. Assuming the dipole−dipole interactions to be dominant within as well as between stacks, i.e., a $1/r^6$ dependence for the corresponding E.T. rate constants, a $(k^x_{ET}/k^y_{ET})^{1/6}$ ratio of ≈1.6 follows from M.C. simulations. Using the extended dipole approximation[60] for the dipole−dipole interactions, the lower limit of the ratio $(k^x_{ET}/k^y_{ET})^{1/6} \approx (r^x/r^y)$ for the closely packed structure is found to be ≈1.6. Although the calculated ratio of the corresponding E.T. is rather approximate, it obviously indicates a closer relation with the Förster type of E.T. than that with exchange E.T., which should result in a much large ratio.

Finally, all E.T. parameters obtained from the M.C. simulation-based analysis for **system 1** support previously reported results.[30]

4.2. System 2. *4.2.1. Structure.* The porphyrin tetramer of **system 2** results from self-organization of Zn(4-Py)TrPP in toluene at 10 °C[33] as shown in Figure 8. Since energy transfer between the identical porphyrin units in the tetramer does not affect the fluorescence lifetime, the only way to obtain information on E.T. within the tetramer is to analyze the time dependence of the fluorescence anisotropy, following a polarized excitation pulse.

4.2.2. Simulation Model. The simulation model of **system 2** assumes the [ZnM(4-Py)TrPP]$_4$ aggregate to consist of four mutually ligated porphyrins bound in such way that each molecule is perpendicular to the plane of a neighboring one. A schematic diagram of E.T. pathways in the tetramer is shown

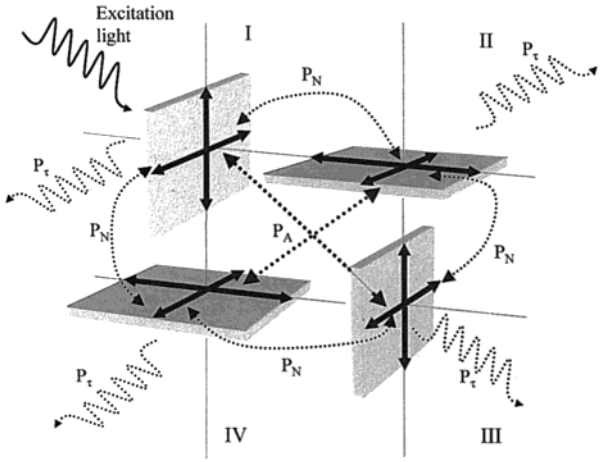

Figure 9. Schematic diagram of the energy transfer pathways in the $[ZnM(4\text{-}Py)TrPP]_4$ tetramer. For meaning of symbols, see text.

in Figure 9. At the start of a simulation run the coordinate system of the tetramer is randomly generated in the laboratory coordinate system. If the molecules in the tetramer are numbered as 1, 2, 3, and 4 then all possible molecular pairs involved in E.T. are labeled *ij*, where $i = 1, 2, 3,$ and 4 and $j = 1, 2, 3,$ and 4, $i \neq j$. The parameters k^{ij}_{ET} represent the rate constants for energy transfer between the ith and jth molecules in the tetramer; and τ is the ZnM(4-Py)TrPP fluorescence lifetime. If we assume that $k^{ij}_{ET} = k^{ji}_{ET}$, then all possible E.T. steps in the tetramer can be reduced to two parameters: k^N_{ET} for E.T. between nearest neighbors and k^A_{ET} for E.T. between next-nearest neighbors, i.e., between a pair of molecules across the tetramer. The parameters k^N_{ET}, k^A_{ET}, and τ^{-1} are proportional to the probabilities P^A_{ET}, P^N_{ET}, and P_τ (where $P^A_{ET} + P^N_{ET} + P_\tau = 1$), to be used in the simulation model. A flow diagram of the simulation model of E.T. in **system 2** is presented in Appendix B.

4.2.3. Results and Discussion of Computer Simulations. The monomer porphyrins were excluded from the simulation, as their fraction is negligibly small under the conditions of the experiment (10 °C, $\lambda_{exc} = 565$ nm and $\lambda_{det} = 616$ nm). Energy transfer between the tetramers and singlet−singlet annihilation are not included in the simulations considering the low concentration (10^{-5} M) and excitation rate, respectively. Since the analysis uses a 160 ps time window and $(k^N_{ET})^{-1}$ and $(k^A_{ET})^{-1} \ll \phi_{tetr} \sim 1$ ns[33], the rotational diffusion of the tetramers is not taken into consideration. The experimental fluorescence anisotropy decay of the porphyrin tetramers was analyzed using parametric fitting by the M.C. simulation model for **system 2**, described above.

Using 999 channels with 0.2 ps per channel for the simulated histograms, the fluorescence anisotropy decay could be fitted well by the simulated decay using 10^7 simulation runs. Figure 10 shows typical fits of the experimental anisotropy decay with the following parameters: $k^N_{ET} = 38 \times 10^9$ s^{-1}, $k^A_{ET} = 5 \times 10^9$ s^{-1}, and $\tau = 1.50$ ns (Table 1).

As expected, E.T. between neighboring porphyrins is much faster than across the tetramer, which explains the fast depolarization in the initial part of the anisotropy decay. The E.T. parameters obtained by the M.C. simulations agree with the values of $(31 \pm 2) \times 10^9$ s^{-1} and $(5.3 \pm 0.3) \times 10^9$ s^{-1} calculated from Förster theory using the point dipole−dipole model.[33] The calculated value of 31×10^9 s^{-1} is close to that of the short component of $\sim 38 \times 10^9$ s^{-1} found by the M.C. simulations, whereas the calculated value of 5.3×10^9 s^{-1} equals the longer one from the simulation. Note, however, that the lower boundary of the 95% confidence interval of k^A_{ET} is

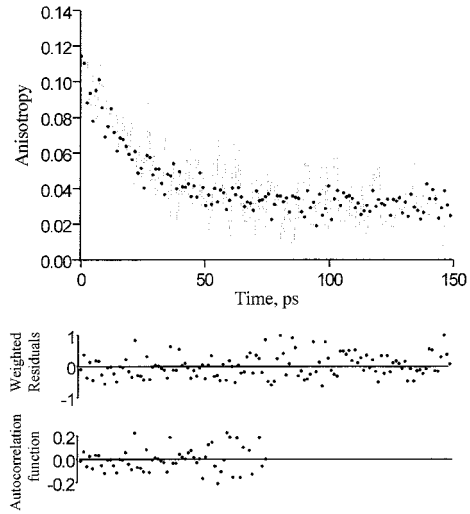

Figure 10. Example of simulation-based fit (●, $\chi^2 = 1.01$) of the experimental $[ZnM(4\text{-}Py)TrPP]_4$ fluorescence anisotropy decay (−). $\lambda_{exc} = 565$ nm; $\lambda_{det} = 616$ nm.

undefined between the upper boundary and zero in the detection window of 160 ps.

We have also checked the influence of monomer deformation in the tetramer on the E.T. rate constants by optimizing the angle between the degenerated absorption and emission monomer transition dipole moments. Introducing the angle η as half of the angle between the degenerate moments, eqs 17 and 18 of Appendix B become

$$P_{I_\parallel} \sim 3/2\,(1 - \sin^2\alpha \sin^2\phi)\,(\cos\phi \cos\alpha \cos\xi \sin\eta - \sin\phi \sin\xi \sin\eta + \cos\phi \sin\alpha \cos\eta)^2 \quad (11)$$

$$P_I\perp \sim {}^3/_2\,(1 - \sin^2\alpha \sin^2\phi)\,(-\sin\alpha \cos\xi \sin\eta + \cos\alpha \cos\eta)^2 \quad (12)$$

Deformation of the monomers bound into the tetramer may influence the rate constants for both abovementioned E.T. processes by changing the relative contribution to these rate constants by the dipole−dipole and exchange mechanism. The best fit has been found when the porphyrins are completely flat in the tetramer, i.e., the angle between the degenerate moments is 90°. A ±1° deviation of this angle leaves other parameters in the 95% confidence intervals. The distortions of the tetramer, resulting from rotation of the monomers, are omitted since the steady state optical spectra of the tetramers indicate that the bound monomers are mutually perpendicular.[33]

This work demonstrates that M.C. simulation of the energy transfer processes in self-organized $[Zn(4\text{-}Py)TrPP]_4$ tetramers and ZnTOPP films, using a physical model of their structure and excited state kinetics, can successfully extract the relevant kinetic parameters from the experimental complex fluorescence and fluorescence anisotropy decays of the film. For both systems the E.T. rate constants resulting from M.C. simulations are in accordance with the corresponding aggregate structures, i.e., a domain of ordered stacks[56,57] for **system 1** and a cyclic tetramer for **system 2** and E.T. of the Förster type. The results of the M.C. simulations show that E.T. of the exchange type can be neglected for both systems.

An important point concerns the problem that the M.C. simulation analysis may result in a local minimum. In general, an adequate determination of the parameters requires a check

of their confidence intervals by the exhaustive search method.[61] It is impractical, however, to apply this precise method to the M.C. simulation analysis using a PC, since this would result in a dramatic increase of the processing time. We used the less time-consuming, but also less accurate asymptotic standard errors method[59] to approximate the confidence intervals of the parameters resulting from M.C. simulation. The use of global analysis considerably reduces the risk of reaching local minima, however.

The M.C. simulation-fitting method is not limited to the processes or systems investigated in this work, but is expected to be equally effective for other more complex systems showing nonisotropic E.T. and/or different processes involving excited states.

5. Conclusions

An improved type of analysis of time-resolved fluorescence data by means Monte Carlo simulations, i.e., direct fitting of the experimental fluorescence and anisotropy decays, has been developed and successfully demonstrated for two differently organized porphyrin systems;

Two energy transfer constants, i.e., $\sim 1 \times 10^{12}$ and $\sim 80 \times 10^9$ s^{-1} assigned to intra- and inter-stack transfer, respectively, and a $\sim 0.6 \times 10^{-2}$ molar fraction of nonintentional impurity were found in thin, undoped films of zinc tetra-(octylphenyl)-porphyrin. The ratio $(k^x_{ET}/k^y_{ET})^{1/6} \approx 1.6$ of these rate constants agrees with the theoretical ratio ($\approx$1.6) calculated from the domain structure of ZnTOPP stacks in the film and a Förster type of energy transfer;

Using the Monte Carlo method, the E.T. rate constants were calculated for porphyrin tetramers to be 38×10^9 and 5×10^9 s^{-1}. These values agree with a Förster type of E.T. yielding 31×10^9 and 5.3×10^9 s^{-1} for transfer to nearest and next-nearest neighbors and support the model of a highly symmetrical tetramer in which the porphyrins are not distorted from the D_{4h} symmetry and are perpendicularly oriented by intermolecular ligation. In this structure intermolecular exchange interactions can be safely neglected.

Acknowledgment. We are grateful to Drs. S. Gobets, Dr. I. van Stokkum, and Professor R. van Grondelle (Free University, Amsterdam) for making available the streak camera instrumentation and for their help with the measurements.

Appendix A

A flow diagram for a single simulation run for **system 1** is presented in Figure 11, and can be considered as a subroutine of **block 2** in Figure 4. The molecular sites in the x and in y directions are counted by $i = 1,...,1000$ and $j = 1,...,200$, respectively. The position (i_0,j_0) of the first excited molecule, the positions (i^l,j^l), $l = 1,...,1000N_{CuTOPP}$ of the N_{CuTOPP} dopant molecules and the positions (i^k,j^k), $k = 1,..., 1000N_{imp}$ of N_{imp} impurity molecules are randomly generated at the start of every simulation run (**block 1**). Since the ZnTOPP domain can be considered as a homogeneous system, and to keep the excitation within a domain, we used the so-called "mirror rejection" for the boundary conditions. Subsequently, the fluorescence emission events and E.T. steps in the x and y directions are simulated in **block 3** using a discrete probability distribution, defined by P^x_{ET}, P^y_{ET}, and P_τ, using a random number R, uniformly distributed in the interval [0;1], and generated in **block 2**. The time required for a single of energy transfer step can be considered to be a continuous, random variable, distributed exponentially. Thus, the time Δt of E.T. from one molecule to another is given by[7]

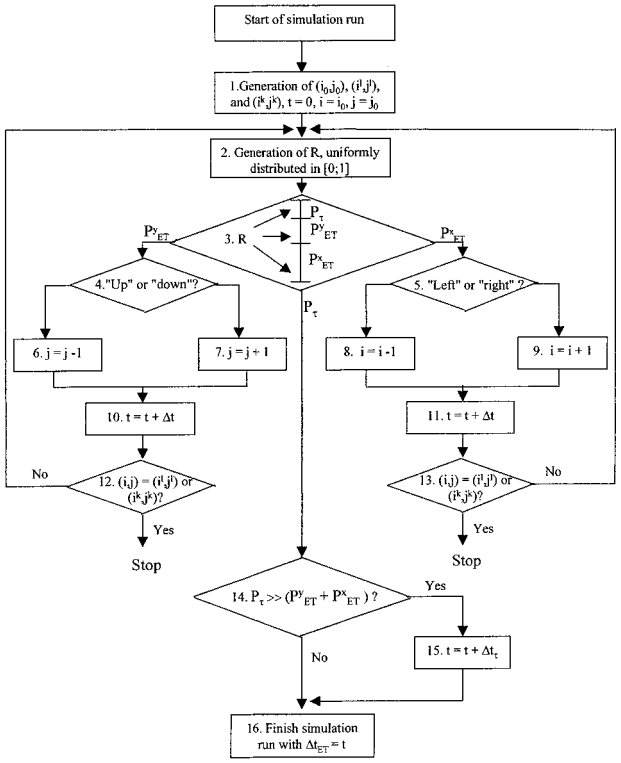

Figure 11. Flow diagram of one simulation run in **system 1**.

$$\Delta t = -(k^q_{ET})^{-1} \ln(R) \qquad (13)$$

where q represents either x or y, depending on the direction of the hop, and R is a new random number, uniformly distributed in the interval [0;1]. Random traveling of excitation energy through the system is simulated in **blocks 2**−**11** until it is emitted or trapped by the dopant or impurity molecule in **blocks 12**−**16**. Upon trapping by an impurity, the excitation energy walk stops without registering Δt_{ET} in **block 14**−**16**, i.e., without emission of the photon.

Appendix B

A flow diagram of the simulation model of E.T. in **system 2** is presented in Figure 12. This diagram represents in fact a subroutine of **block 2** in Figure 4. An E.T. walk starts (**block 1)** by generating the number i_0 of the initially excited molecule and its orientation $\Omega = (\alpha,\phi,\xi)$ with respect to the laboratory coordinate system. Note that for a given tetramer structure Ω also defines the orientation of the tetramer.

The emission transition dipoles of metallo-porphyrins are degenerate and mutually perpendicular, since the porphyrin macrocycle has D_{4h} symmetry. The orientation of the porphyrin monomer is then defined by three angles. For example, if α and ϕ are the spherical coordinates of either one of the degenerate emission moments with respect to the laboratory coordinate system, then ξ is a third angle defining the orientation of the molecular coordinate system with respect to that of the laboratory.

Following **block 2** the events of fluorescence emission or E.T. are simulated in **block 3** using a random number R, uniformly distributed in the interval [0;1], as generated in **block 2** and the probabilities P^A_{ET}, P^N_{ET}, and P_τ. Again, the actual excitation event is considered to be instantaneous. The time Δt at which the excitation is localized on the ith molecules is

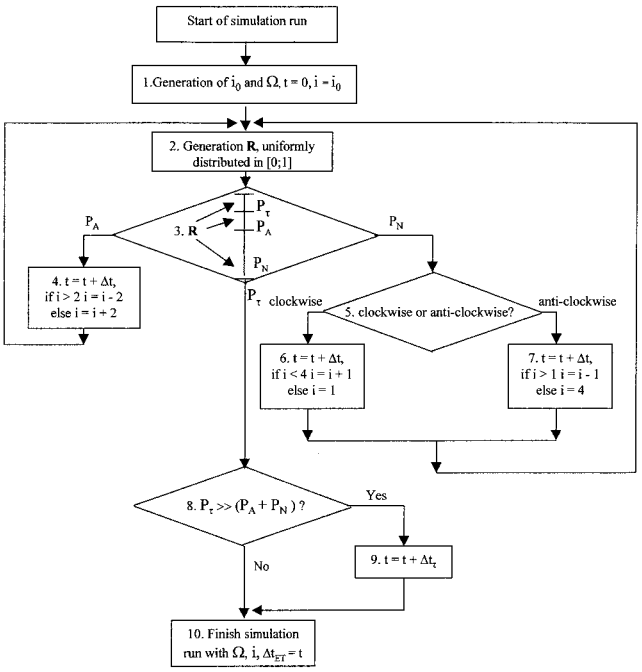

Figure 12. Flow diagram of one simulation run in s**ystem 2**.

given by[7]

$$\Delta t = -(k^q_{ET})^{-1} \ln(R) \quad (14)$$

where $q = N$ or A, and R is a new random number, uniformly distributed in the interval [0;1]. The simulation of E.T. is repeated in **blocks 2−7** until the event of the fluorescence emission is generated. After each simulation run the total time Δt_{ET} after multiple hops is recorded as histograms of the "parallel component" ($P_{I||}$) or the "perpendicular component" ($P_I\perp$), where "parallel" and "perpendicular" refer to the orientation of the last molecule participating in the E.T. chain. Then, for the initially excited and next nearest porphyrin within the tetramer, eqs 9 and 10 can be rewritten as

$$P_{I_{||}} \sim {}^3/_4(1 - \sin^2\alpha \sin^2\phi)\,(\cos\phi \cos\alpha \cos\xi - \sin\phi \sin\xi + \cos\phi \sin\alpha)^2 \quad (15)$$

$$P_I\perp \sim {}^3/_4(1 - \sin^2\alpha \sin^2\phi)(-\sin\alpha \cos\xi + \cos\alpha)^2 \quad (16)$$

and for the nearest neighbors to the left and right of the initially excited porphyrin unit, eqs 9 and 10 are

$$P_{I_{||}} \sim {}^3/_8(1 - \sin^2\alpha \sin^2\phi)\,(\sqrt{3}\cos\phi \cos\alpha \cos\xi - \sqrt{3}\sin\phi \sin\xi + \cos\phi \sin\alpha)^2 \quad (17)$$

$$P_I\perp \sim {}^3/_8(1 - \sin^2\alpha \sin^2\phi)\,(-\sqrt{3}\sin\alpha \cos\xi + \cos\alpha)^2 \quad (18)$$

References and Notes

(1) Michel-Beyerle, M. E., Ed. *Antennas and Reaction Centers in Photosynthetic Bacteria*; Springer-Verlag: Berlin, 1985.

(2) Breton, J.; Vermeglio, H. *The Photosynthetic Bacterial Reaction Center: Structure and Dynamics*; Plenum Press: New York, 1988.

(3) Quillec, M., Ed. *Materials for Optoelectronics*; Kluwer Academic Publishers: Boston, 1996.

(4) Donati, S. *Photodetectors, Devices, Circuits and Applications*; Prentice Hall: New Jersey, 2000.

(5) Chopra, K. L.; Das, S. R. *Thin Film Solar Cells*; Plenum Press: New York, 1983.

(6) Agranovich, V. M.; Galanin, M. D. *Electronic Excitation Energy Transfer in Condensed Matter*; North-Holland: New York, 1982.

(7) Andrews, L.; Demidov, A., Eds. *Resonance Energy Transfer*; John Wiley & Sons Ltd., Inc.: New York, 1999.

(8) Lakowicz, J. R. *Principles of Fluorescence Spectroscopy*, 4th ed.; Kluwer Academic/Plenum Publishers: New York, 1999.

(9) Giggino, K. P.; Smith, T. A. *Prog. React. Kinet.* **1993**, *18*, 375.

(10) Markovitsi, D.; Germain, A.; Millié, P.; Lécuyer, P.; Gallos, L. K.; Argyrakis, P.; Bengs, H.; Ringsdorf, H. *J. Phys. Chem.* **1995**, *99*, 1005.

(11) Bacchiocchi, C.; Zannoni, C. *Chem. Phys. Lett.* **1997**, *268*, 541.

(12) Berberan-Santos, M. N.; Choppinet, P.; Fedorov, A.; Jullien, L.; Valeur, B. *J. Am. Chem. Soc.* **1999**, *121*, 2526.

(13) Sato, N.; Ito, S.; Sugiura, K.; Yamamoto, M. *J. Phys. Chem. A* **1999**, *103*, 3402.

(14) Loura, L. M. S.; Prieto, M. *J. Chem. Phys. B* **2000**, *104*, 6911.

(15) Rubinstein, R.; Shapiro, A. *Modern Simulation and Modeling*; John Wiley & Sons Ltd., Inc.: New York, 1998.

(16) Binder, K.; Heerman, D. V. *Monte Carlo Simulation in Statistical Physics*; Springer-Verlag: Berlin, 1992.

(17) Harvey, S. C.; Cheung, H. C. *Proc. Natl. Acad. Sci. U.S.A.* **1972**, *69*, 3670.

(18) Berberan-Santos, M. N.; Valeur, B. *J. Chem. Phys.* **1991**, *95*, 8049.

(19) Johansson, L. B. Å.; Engström, S.; Lindberg, M. *J. Phys. Chem.* **1992**, *96*, 3845.

(20) Hussey, D. M.; Matzinger, S.; Fayer, M. D. *J. Chem. Phys.* **1998**, *109*, 8708.

(21) Förster, T. *Ann. Phys.* **1948**, *2*, 55.

(22) Dexter, D. L. *J. Chem. Phys.* **1953**, *21*, 836.

(23) Apanasovich, V. V.; Novikov, E. G.; Yatskov, N. N. *Proc. SPIE* **1997**, *2980*, 495.

(24) Apanasovich, V. V.; Novikov, E. G.; Yatskou, M. M. *J. Appl. Spectrosc.* **2001**. In press.

(25) Kerp, H. R.; Donker, H.; Koehorst, R. B. M.; Schaafsma, T. J.; van Faassen, E. E. *Chem. Phys. Lett.* **1998**, *298*, 302.

(26) Lawrence, D.; Jiang, I.; Levett, M. *Chem. Rev.* **1995**, *95*, 2229.

(27) Prodi, A.; Indelli, M. T.; Kleverlaan, C. J.; Scandola, F.; Alessio, E.; Gianferrara, T.; Marzilli, L. G. *Chem. Eur. J.* **1999**, *5*, 2668.

(28) Li, F.; Gentemann, S.; Kalsbeck, W. A.; Seth, J.; Lindsey, J. S.; Holten, D.; Bocian, D. F. *J. Mater. Chem.* **1997**, *7*, 1245.

(29) Cho, H. S.; Song, N. W.; Kim, Y. H.; Jeoung, S. C.; Hahn, S.; Kim, D.; Kim, S. K.; Yoshida, N.; Osuka, A. *J. Phys. Chem. A* **2000**, *104*, 3287.

(30) Donker, H.; Koehorst, R. B. M.; van Hoek, A.; van Schaik, W.; Schaafsma, T. J. *J. Phys. Chem. B* **2001**. Submitted for publication.

(31) Dlott, D. D.; Fayer, M. D.; Wieting, R. D. *J. Chem. Phys.* **1977**, *67*, 3808.

(32) Wieting, R. D.; Fayer, M. D.; Dlott, D. D. *J. Chem. Phys.* **1978**, *69*, 1996.

(33) Yatskou, M. M.; Donker, H.; Koehorst, R. B. M.; van Hoek, A.; Schaafsma, T. J. *J. Phys. Chem. A* **2001**. Submitted for publication.

(34) Engström, S.; Lindberg, M.; Johansson, L. B. Å. *J. Phys. Chem.* **1988**, *89*, 204.

(35) Baumann, J.; Fayer, M. D. *J. Chem. Phys.* **1986**, *85*, 4087.

(36) Enrenberg, A. S. C. *Data Reduction*; John Wiley & Sons Ltd., Inc.: New York, 1975.

(37) Korn, G. A.; Korn, T. M. *Mathematical Handbook for Scientists and Engineers*; McGraw- Hill Book Company: New York, 1961.

(38) O'Connor, D. V.; Phillips, D. *Time-Correlated Single Photon Counting*; Academic Press: London, 1984.

(39) Demas, J. N. *Excited-State Lifetime Measurements*; Academic Press: New York, 1983.

(40) Barlow, R. *J. Comput. Phys.* **1987**, *72*, 202.

(41) Barlow, R.; Beeston, C. *Comput. Phys. Commun.* **1993**, *77*, 219.

(42) Ameloot, M.; Hendrix, H. *J. Chem. Phys.* **1982**, *76*, 4419.

(43) Chowdhury, F. N.; Kolber, Z. S.; Barkley, M. D. *Rev. Sci. Instrum.* **1991**, *62*, 47.

(44) Beechem, J.; Ameloot, M.; Brand, L. *Chem. Phys. Lett.* **1985**, *120*, 446.

(45) Bratley, P.; Fox, B. L.; Schrage, L. E. *A Guide to Simulation*; Springer: New York, 1983.

(46) Lakowicz, J. R., Ed. *Topics in Fluorescence Spectroscopy*; Plenum Press: New York, 1991; Vol. 2.

(47) Adler, A. D.; Longo, F. R.; Kampas, F.; Kim, J. *J. Inorg. Nucl. Chem.* **1970**, *32*, 2443.

(48) Adler, A. D.; Longo, F. R.; Shergalis, W. *J. Am. Chem. Soc.* **1964**, *86*, 3145.

(49) Little, R. G.; Anton, J. A.; Loach, P. A.; Ibers, J. A. *J. Heterocycl. Chem.* **1975**, *12* 343.

(50) Visser, A. J. W. G.; van den Berg, P. A. W.; Visser, N. V.; van Hoek, A.; van den Burg, H. A.; Parsonage, D.; Claiborne, A. *J. Phys. Chem. B* **1998**, *102*, 10431.

(51) van den Berg, P. A. W.; van Hoek, A.; Walentas, C. D.; Perham, R. N.; Visser, A. J. W. G. *Biophys. J.* **1998**, *74*, 2046.

(52) van Hoek, A.; Visser, A. J. W. G. *Rev. Sci. Instrum.* **1981**, *52*, 1199.

(53) Vos, K.; van Hoek, A.; Visser, A. J. W. G. *Eur. J. Biochem.* **1187**, *165*, 55.
(54) van Hoek, A.; Visser, A. J. W. G. *Anal. Instrum.* **1985**, *14*, 359.
(55) Gobets, B.; van Stokkum, I. H. M.; Rögner, M.; Kruip, J.; Kleima, F. J.; Schlodder, E.; Karapetyan, N. V.; Dekker: J. P.; van Grondelle, R. *Biophys. J.*, submitted.
(56) Shimizu, Y.; Miya, M.; Nagata, A.; Ohta, K.; Yamamoto, I.; Kusabayashi, S. *Liq. Cryst.* **1993**, *14*, 795.
(57) Shimizu, Y.; Higashiyama, T.; Fuchita, T. *Thin Solid Films* **1998**, *331*, 279.
(58) Nelder, J. A.; Mead, R. *Comput. J.* **1965**, *8*, 308.
(59) Johanson, M. J. *Methods Enzymol.* **1994**, *240*, 1.
(60) Czikklely, V.; Forsterling, H. D.; Kuhn, H. *Chem. Phys. Lett.* **1970**, *6*, 207.
(61) Beechem, J. M. *Methods Enzymol.* **1992**, *210*, 37.